ELSEVIER

Journal of Alloys and Compounds 358 (2003) 235–244

Journal of ALLOYS AND COMPOUNDS

www.elsevier.com/locate/jallcom

Syntheses, structures and luminescent properties of Sm (III) and Eu (III) chelates for organic electroluminescent device applications

Y.J. Fu[a], T.K.S. Wong[a,*], Y.K. Yan[b], X. Hu[c]

[a]*Division of Microelectronics, School of Electrical & Electronic Engineering, Nanyang Technological University, Singapore 639798, Singapore*
[b]*Natural Sciences Academic Group, National Institute of Education, Nanyang Technological University, 1 Nanyang Walk, Singapore 637616, Singapore*
[c]*Division of Materials Technology, School of Materials Engineering, Nanyang Technological University, Singapore 639798, Singapore*

Received 1 April 2002; received in revised form 1 November 2002; accepted 12 December 2002

Abstract

Samarium(III) and europium(III) complexes of the β-diketone ligand (2-thienyl)trifluoroacetylacetone (HTTA) and triphenylphosphine oxide (TPPO) were prepared. The complexes, $Sm(TTA)_2(TPPO)_2NO_3$ (**1**), $Eu(TTA)_2(TPPO)_2NO_3H_2O$ (**2**), and $Eu(TTA)_3(TPPO)_2$ (**3**) were characterized. Single crystal X-ray diffraction molecular structures of complexes **1** and **3** are presented and some of the crystal parameters for complex **1** are: space group, *P*1; $a = 11.019(4)$ Å, $b = 11.791(6)$ Å, $c = 12.535(5)$ Å; $\alpha = 102.68(3)°$, $\beta = 102.06(3)°$, $\gamma = 117.75(3)°$; for complex **3**: space group, $P-1$, $a = 11.1946(9)$ Å, $b = 12.117(2)$ Å, $c = 23.535(2)$ Å, $\alpha = 80.047(13)°$, $\beta = 76.498(7)°$, $\gamma = 70.450(9)°$. Electroluminescent devices were fabricated by vacuum evaporation. Apart from single layer devices, double and triple layer devices with the following structures: ITO/TPD/Complex **2**/Al; ITO/TPD/Complex **3**/Al; ITO/TPD/Complex **2**/Alq/Al were studied, where *N*,*N*-bis(3-methylphenyl)-*N*,*N*′-diphenyl-benzidine (TPD) was used as a hole transporting layer and tris(8-hydroxyquinolinate)aluminum (Alq) as an electron transporting layer. The results indicate that single layer devices show very low quantum efficiency, while the double layer devices with a hole transporting layer exhibit enhanced efficiency and a well defined EL spectrum. No significant improvement was observed in the triple layer devices with an additional electron transporting layer.

Keywords: Thin films; Crystal structure and symmetry; Luminescence; Thermal analysis

1. Introduction

Organic light emitting devices (OLEDs) are considered promising for applications in new types of flat panel displays since the first reports by Tang and VanSlyke [1,2] on the highly efficient electroluminescence (EL) from organic thin-films. In these systems, holes and electrons injected from electrodes recombine and light is emitted from excited molecules in the luminescent layer as a result of exciton decay. Fluorescent dyes, conjugated polymers and metal complexes are the three main categories of organic EL materials. Among the metal chelates, tris(8-hydroxyquinolinate) aluminum (Alq) is the most extensively studied both as a green emitter and as an electron transporting material. It has been pointed out in an earlier review article that in order for chelate complexes to be vacuum evaporated in OLED fabrication, they must be of the inner salt type [3]. This means the chelates should be neutral molecules and no ionic bonding force should exist. Apart from Al(III), other metal ions used in OLEDs include: B(III), Ga(III), In(III), Mg(II), Be(II), Zn(II), Ru(II), Eu(III), Eu(II), Tb(III), Er(III), Dy(III) [3–17]. Chelate complexes based on rare earth (lanthanide) ions and organic ligands are especially significant because of their many desirable photophysical characteristics. Unlike transition metal complexes, the electroluminescence efficiency of rare earth chelates is not limited to a theoretical maximum of 25% of the photoluminescence efficiency. High efficiency red emitting devices have been reported by Hong et al. [18] and Adachi [19]. In general, it is difficult to obtain pure emission colors from conjugated polymers and small organic molecules because of their broad emission spectra (50–200 nm) [20]. Narrow band EL emission in the red, green, blue and white colors have been observed in Eu^{3+}, Tb^{3+}, Tm^{3+} and Dy^{3+} complexes [20–22]. The availability of pure emission colors is important for full color organic flat panel displays. In

*Corresponding author. Tel.: +65-679-064-01; fax: +65-679-204-15.
E-mail address: ekswong@ntu.edu.sg (T.K.S. Wong).

0925-8388/03/$ – see front matter
doi:10.1016/S0925-8388(03)00047-1

addition, rare earth complexes allow the color, efficiency and device lifetime to be simultaneously optimized [23]. This is because the emission color is determined by the rare earth ion while the chelating ligands determine other physical characteristics [24]. The above mentioned characteristics arise because compared to other luminescent materials, the rare earth chelates have two distinctive features: (1) they exhibit extremely sharp emission bands arising from transitions between f^n levels with the effective shielding effect of the overlying $5s^2$ and $5p^6$ orbits [5,6]; (2) up to 100% of internal device quantum efficiency is theoretically possible since the metal ions are excited via intramolecular energy transfer from the triplet excited state of the ligands and both the singlet state and triplet state excitation energy can be utilized to excite the emitting center. It is because of these features that rare earth chelates have attracted and will continue to attract much attention in the field of OLEDs. Europium (III) and terbium (III) complexes are the most extensively studied as red and green emission materials. Device luminance of 820 cd/m^2 [14] and 920 cd/m^2 [15] were reported respectively for Eu(III) and Tb(III) based devices. However, amongst the numerous reports, synthesis and molecular structures of the rare earth chelates are rarely studied in detail. In this paper, we report results of a study on the synthesis, characterization, and luminescent properties of several rare earth complexes.

2. Experimental

2.1. Materials preparation

Complex **1**: Samarium(III) nitrate, $Sm(NO_3)_3 6H_2O$ (44.4 mg, 0.1 mmol) was dissolved in 20 ml methanol. This solution was added slowly into a mixed solution of (2-thienyl) trifluoro-acetylacetone (HTTA) (66.6 mg, 0.3 mmol) and triphenylphosphine oxide (TPPO) (55.6 mg, 0.2 mmol) in 20 ml methanol with stirring. The solvent was allowed to evaporate and the product was obtained in the form of a white powder with a yellow hue.

Complex **2** was prepared and purified by a similar process as complex **1**, except that europium(III) nitrate, $Eu(NO_3)_3 5H_2O$ (42.8 mg, 0.1 mmol) was used instead of $Sm(NO_3)_3 6H_2O$. The product obtained was a pink powder.

Complex **3** was prepared by a similar process as above except that europium(III) acetate, $Eu(OAc)_3 xH_2O$ was used. The product was a yellow powder with a pink hue.

The materials were further purified by recrystallization from a methanol/*iso*-propanol mixture. Single crystals of complexes **1** and **3** suitable for X-ray diffraction analysis were obtained through slow evaporation of the mixed solvent. However attempts to obtain good quality single crystals for complex **2** were unsuccessful due to rapid desolvation of crystals upon removal from the mother liquor.

2.2. Characterization

2.2.1. X-ray crystallography

X-ray diffraction analyses were carried out for complexes **1** and **3**. Crystal data and parameters for data collection and refinement are summarized in Table 1, while selected bond lengths and angles are listed in Table 2. Further data is available upon request.

The reflection data was collected on a Siemens P4 four-circle diffractometer with graphite-monochromated Mo Kα radiation ($\lambda = 0.71073$ Å) at 298(2) K using the θ–2θ scan mode. A semi-empirical absorption correction from Ψ scans was applied. The structures were solved by direct methods for complex **1** and the heavy atom method for complex **3** and were refined on F^2 by full-matrix least-squares methods using the SHELXTL Plus package [25]. All the non-hydrogen atoms (except the carbon atoms of the two TTA ligands of complex **1**) were refined anisotropically. As for the hydrogen atoms, they were placed in calculated positions (C–H 0.96 Å) and were assigned fixed isotropic thermal parameters at 1.2 times the equivalent isotropic U of the atoms to which they are attached and allowed to ride on their respective parent atoms. The contributions of these hydrogen atoms were included in the structure–factor calculations. The absolute structure of complex **1** was determined by the refinement of the Flack parameter [26].

2.2.2. Thermogravimetric analysis (TGA) and differential scanning calorimetry (DSC) measurements

TGA and DSC measurements were carried out under nitrogen gas using a Hi-Res TGA 2950 thermogravimetric analyzer and a DSC 2010 differential scanning calorimeter respectively.

2.2.3. Photoluminescence (PL) and electroluminescence (EL) measurement

In the fabrication of EL devices, indium–tin oxide (ITO)-coated glass (60 Ω/square), was cut and patterned in concentrated hydrochloric acid and then ultrasonically cleaned for 10 min in detergent, de-ionized water, acetone and methanol respectively in sequence. The ITO glass was used as the anode of the OLEDs. For single layer devices, an organic layer of the complex and the Al electrode were evaporated sequentially at pressures below 2×10^{-6} Torr inside a vacuum evaporator onto the ITO-coated glass substrate. The double layer devices were fabricated in a similar procedure except that a *N*,*N*-bis(3-methylphenyl)-*N*,*N*′-diphenylbenzidine (TPD) layer was first evaporated on the ITO glass before the evaporation of the complex. The triple layer devices were fabricated with the addition

Table 1
Crystal data and structural refinement for complexes **1** and **3**

	Complex **1**	Complex **3**
Empirical formula	$C_{52}H_{38}F_6NO_9P_2S_2Sm$	$C_{60}H_{42}F_9O_8P_2S_3Eu$
Formula weight	1211.24	1372.02
System	Triclinic	Triclinic
Space group	$P1$	$P-1$
a (Å)	11.019(4)	11.1946(9)
b (Å)	11.791(6)	12.117(2)
c (Å)	12.535(5)	23.535(2)
α(°)	102.68(3)	80.047(13)
β(°)	102.06(3)	76.498(7)
γ(°)	117.75(3)	70.450(9)
Volume (Å^3)	1311.7(10)	2909.6(5)
Z	1	2
D_{calc}(Mg/m^3)	1.533	1.566
Absorption coefficient (mm^{-1})	1.336	1.324
F(000)	607	1376
θ range(°)	1.79–25.00	1.79–25.00
Limiting indices	$-1 \le h \le 9$	$-12 \le h \le 1$
	$-12 \le k \le 11$	$-14 \le k \le 13$
	$-14 \le l \le 14$	$-27 \le l \le 27$
Reflections collected	4313	11841
Independent reflections	4313 [$R_{int} = 0.0000$]	10138 [$R_{int} = 0.0298$]
T_{max} and T_{min}	0.8165 and 0.5148	0.7786 and 0.6546
Data/parameters	4249/578	9909/749
Goodness-of-fit on F^2	1.040	1.022
R indices [$I > 2\theta(I)$] R_1	0.0681	0.0318
wR_2	0.1661	0.0827
R indices (all data) R_1	0.0810	0.0379
wR_2	0.1992	0.0909

of a layer of Alq to the double layer structure before Al electrode evaporation.

For PL spectra measurement, quartz was used as the substrate instead of ITO coated glass. All electrical testing and optical measurements were performed under ambient conditions with no encapsulation applied to the devices. Both PL and EL spectra were measured using a RF-5301 PC spectrofluorophotometer.

3. Results and discussion

3.1. Crystal and molecular structures

Fig. 1 shows the molecular structure of complex **1**. In this structure, Sm(III) is coordinated by eight oxygen atoms from the ligands which comprise two TPPO molecules, two $[TTA]^-$ anions and one nitrate anion. The shortest metal–oxygen (M–O) bond lengths occur between Sm(III) and the oxygen atoms from the two TPPO ligands, while the longest ones are between Sm(III) and the two nitrate oxygen atoms, indicating high strain in the four member chelate ring. From the bond angle values, the sum of the four angles, O(3)–Sm(1)–O(4), O(4)–Sm(1)–O(6), O(5)–Sm(1)–O(6), and O(5)–Sm(1)–O(3), equals exactly 360°, so the four oxygen atoms from the two $[TTA]^-$ ions together with Sm(1) exist in the same plane. The other four oxygen atoms, O(1), O(2), O(1N), and O(2N), from the two TPPO molecules and nitrate ion, form another plane (the sum of angles O(1)–Sm(1)–O(2), O(1)–Sm(1)–O(1N), O(1N)–Sm(1)–O(2N), and O(2N)–Sm(1)–O(2) also equals to 360°).

The packing diagram of complex **1** is shown in Fig. 2. The shortest contact distance between molecules exists between an oxygen atom from the nitrate and a sulphur atom from the thiophene groups [O(3N)– S(1), 3.097 Å; O(3N)–S(2), 3.025 Å]. These O–S distances are shorter than the sum of the van der Waals radii of oxygen and sulphur (3.25 Å), and thus may represent weak electrostatic attractions between the partial negative charge on the nitrate oxygen atom and the partial positive charge on the thiophene sulphur atoms. No significant π–π stacking effect between the aromatic rings (i.e. no distance between parallel planes less than 3.5 Å) exists.

As shown in Fig. 3, the Eu(III) ion in complex **3** is coordinated by eight oxygen atoms from two TPPO molecules and three $[TTA]^-$ anions. Thus, in this structure, Eu(III) exhibits a coordination number of 8. Compared with complex **1**, the most significant difference is that an additional $[TTA]^-$ anion coordinates with the metal ion in complex **3** instead of a nitrate ion. From Table 2, we can observe that the differences among the bond lengths in the molecular structure of complex **3** are much smaller than those in the case of complex **1** and no coordination

Table 2
Selected bond lengths (Å) and angles (°) for complexes **1** and **3**

Complex **1**			
Sm(1)–O(1)	2.267(12)	Sm(1)–O(2)	2.314(13)
Sm(1)–O(4)	2.378(12)	Sm(1)–O(3)	2.392(13)
Sm(1)–O(6)	2.399(14)	Sm(1)–O(5)	2.409(13)
Sm(1)–O(1N)	2.48(2)	Sm(1)–O(2N)	2.503(14)
O(1)–Sm(1)–O(2)	155.8(5)	O(1)–Sm(1)–O(4)	94.0(5)
O(2)–Sm(1)–O(4)	94.5(5)	O(1)–Sm(1)–O(3)	82.1(6)
O(2)–Sm(1)–O(3)	79.4(6)	O(4)–Sm(1)–O(3)	70.4(5)
O(1)–Sm(1)–O(6)	95.1(6)	O(2)–Sm(1)–O(6)	92.1(5)
O(4)–Sm(1)–O(6)	142.0(5)	O(3)–Sm(1)–O(6)	147.4(5)
O(1)–Sm(1)–O(5)	79.9(6)	O(2)–Sm(1)–O(5)	80.6(5)
O(4)–Sm(1)–O(5)	146.6(5)	O(3)–Sm(1)–O(5)	76.3(4)
O(6)–Sm(1)–O(5)	71.3(5)	O(1)–Sm(1)–O(1N)	75.7(7)
O(2)–Sm(1)–O(1N)	128.5(7)	O(4)–Sm(1)–O(1N)	73.5(5)
O(3)–Sm(1)–O(1N)	135.8(5)	O(6)–Sm(1)–O(1N)	73.2(5)
O(5)–Sm(1)–O(1N)	134.4(5)	O(1)–Sm(1)–O(2N)	127.3(7)
O(2)–Sm(1)–O(2N)	76.9(7)	O(4)–Sm(1)–O(2N)	74.6(5)
O(3)–Sm(1)–O(2N)	135.5(5)	O(6)–Sm(1)–O(2N)	70.7(5)
O(5)–Sm(1)–O(2N)	134.6(5)	O(1N)–Sm(1)–O(2N)	51.6(6)
O(1)–Sm(1)–N(1)	102.1(8)	O(2)–Sm(1)–N(1)	102.1(7)
O(4)–Sm(1)–N(1)	71.1(5)	O(3)–Sm(1)–N(1)	141.4(4)
O(6)–Sm(1)–N(1)	71.0(5)	O(5)–Sm(1)–N(1)	142.3(5)
O(1N)–Sm(1)–N(1)	26.4(6)	O(2N)–Sm(1)–N(1)	25.3(5)
Complex **3**			
Eu(1)–O(3)	2.364(2)	Eu(1)–O(2)	2.364(2)
Eu(1)–O(7)	2.364(2)	Eu(1)–O(5)	2.368(2)
Eu(1)–O(1)	2.383(2)	Eu(1)–O(8)	2.452(2)
Eu(1)–O(4)	2.452(2)	Eu(1)–O(6)	2.453(2)
O(3)–Eu(1)–O(2)	83.81(9)	O(3)–Eu(1)–O(7)	105.94(9)
O(2)–Eu(1)–O(7)	144.20(8)	O(3)–Eu(1)–O(5)	146.14(8)
O(2)–Eu(1)–O(5)	88.47(9)	O(7)–Eu(1)–O(5)	99.53(9)
O(3)–Eu(1)–O(1)	83.34(9)	O(2)–Eu(1)–O(1)	144.70(8)
O(7)–Eu(1)–O(1)	71.09(8)	O(5)–Eu(1)–O(1)	84.22(9)
O(3)–Eu(1)–O(8)	138.51(8)	O(2)–Eu(1)–O(8)	78.33(8)
O(7)–Eu(1)–O(8)	71.74(8)	O(5)–Eu(1)–O(8)	70.77(8)
O(1)–Eu(1)–O(8)	130.33(9)	O(3)–Eu(1)–O(4)	70.14(8)
O(2)–Eu(1)–O(4)	79.96(9)	O(7)–Eu(1)–O(4)	71.75(9)
O(5)–Eu(1)–O(4)	140.60(8)	O(1)–Eu(1)–O(4)	125.35(9)
O(8)–Eu(1)–O(4)	70.04(8)	O(3)–Eu(1)–O(6)	75.24(8)
O(2)–Eu(1)–O(6)	73.36(8)	O(7)–Eu(1)–O(6)	142.23(8)
O(5)–Eu(1)–O(6)	70.95(8)	O(1)–Eu(1)–O(6)	71.61(8)
O(8)–Eu(1)–O(6)	132.35(8)	O(4)–Eu(1)–O(6)	138.06(8)

plane containing four coordination oxygen atoms and a metal ion exists. Furthermore, the bond lengths between the metal and oxygen atoms from the TPPO in complex **3** are longer than those in complex **1**, indicating a greater steric effect caused by the additional bulky $[TTA]^-$ ions.

3.2. Thermal analysis results

The TGA traces of the three complexes are shown in Fig. 4(a). It can be seen that while the TGA curve of complex **2** shows a weight loss of about 1.5% at 146 °C, those of complexes **1** and **3** are smooth and do not show decomposition until a temperature of about 256 °C is reached when complex **2** also reaches its second decomposition point. The most abrupt weight losses for all three complexes occurred in the temperature range of 256–353 °C leading to similar products, about 20% of the original weight. From these results, the composition of complex **2** is deduced to be $[Eu(TTA)_2(TPPO)_2NO_3(H_2O)]$, with a water content of 1.5% coinciding exactly to the weight loss at 146 °C in the TGA curve. Considering the high tendency for Eu(III) to have a coordination number of nine, the water molecule should be coordinated to the Eu(III) center. The curve of differentiation of weight loss percentage of complex **2** against temperature (also shown in Fig. 4(a)) exhibits a more distinctive change that occurs during the loss of water molecules. The observation that no water or other solvent molecules are incorporated into complex **3** is identical to the single crystal X-ray diffraction analysis results. The

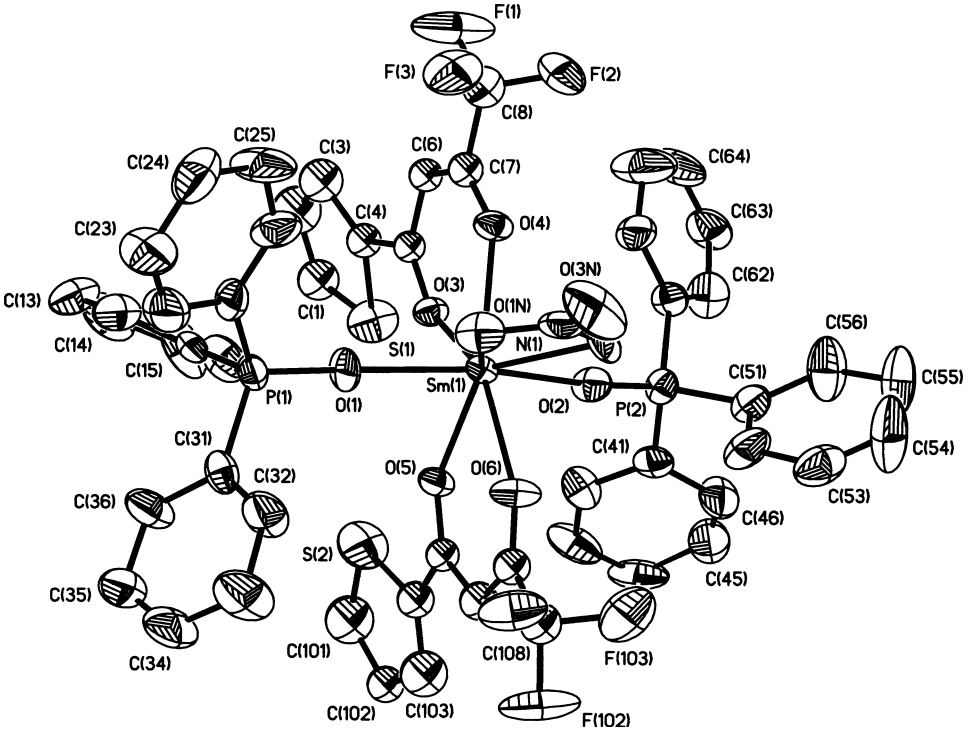

Fig. 1. Molecular structure of complex **1**.

greater steric effect caused by the more bulky ligand, i.e. the third TTA, compared with the smaller-sized nitrate, is probably the reason that the coordination number of Eu(III) in complex **3** is 8 instead of 9 as in complex **2**.

From the DSC curves shown in Fig. 4(b) we can observe that complex **1** melts at 226 °C and complex **3** melts at 169 °C, both with no decomposition before the melting point. It is noteworthy that although the molecular weight of complex **3** is higher, its melting point is lower than that of complex **1**. The lower melting point indicates weaker intermolecular forces in complex **3** and suggests that this complex should be vaporized more easily. The existence of the inorganic nitrate, which has partial negative charge, should be responsible for the higher melting point of complex **1**, as indicated in the lattice packing structure.

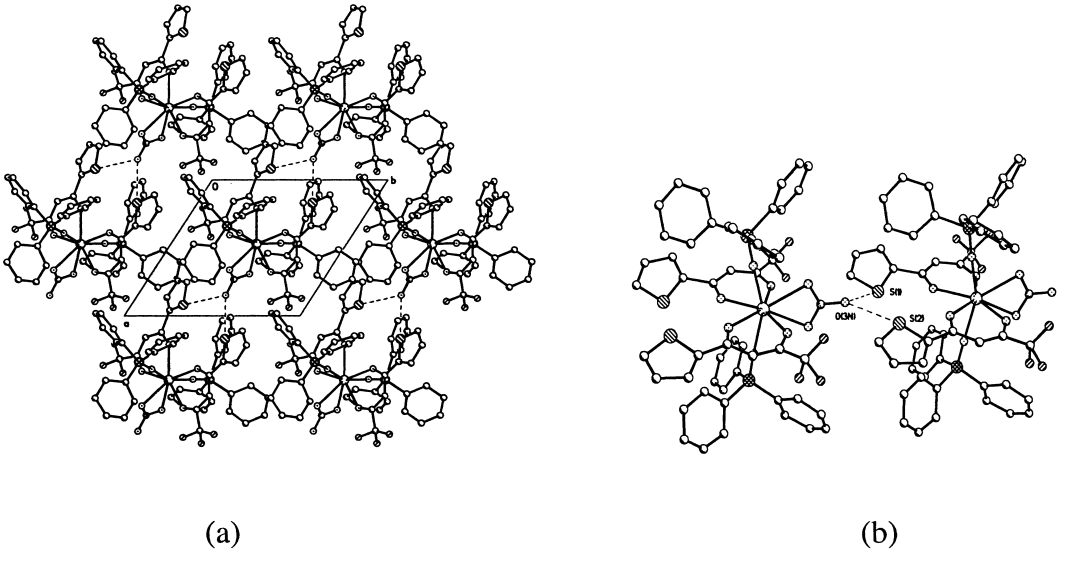

Fig. 2. Packing diagram for complex **1**, viewed down the *c*-axis: dashed lines represent close contacts between O(3N) and S atoms.

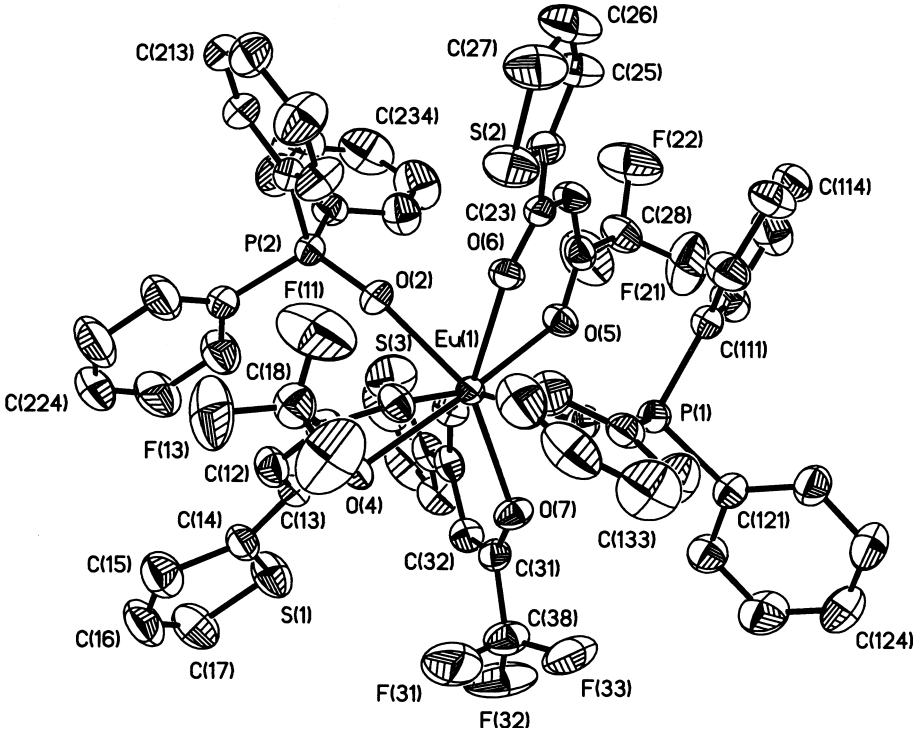

Fig. 3. Molecular structures of complex **3** ($Eu(TTA)_3(TPPO)_2$).

3.3. Factors affecting composition of the materials obtained

We see from the above that three different compositions were obtained in the three cases. This is due to the combined effects of coordination number, acidity, coordination ability and steric effect of the ligands available in the reaction solutions. For the three cases, the reactant HTTA was added according to the same molar ratio of 3:1 to the quantity of rare earth salts. The reactions that occur in the solutions can be formulated as:

$$Sm^{3+} + 2HTTA + 2TPPO + NO_3^- \rightarrow Sm(TTA)_2(TPPO)_2NO_3 + 2H^+ \quad (1)$$

$$Eu^{3+} + 2HTTA + 2TPPO + NO_3^- + H_2O \rightarrow Eu(TTA)_2(TPPO)_2NO_3\,H_2O + 2H^+ \quad (2)$$

$$Eu^{3+} + 3HTTA + 2TPPO + 3OAC^- \rightarrow Eu(TTA)_3(TPPO)_2 + 3HOAC \quad (3)$$

In complexes **1** and **2**, the incorporation of only two TTA^- anions can be explained by the low basicity of the nitrate anion, which does not favor deprotonation of all three HTTA molecules. Solution pH tests showed that the pH values after the reaction was about 1 indicating a high acidity. On the other hand, the acetate anion is much more basic than the nitrate anion, favoring deprotonation of all three HTTA molecules and resulting in pH values greater than 4 in the solution after reaction. Usually pH adjustment was used to prepare rare earth chelates in OLED fabrication. It was reported that from mixed Eu(III) and Gd(III) chloride salts, a composition of $(Eu_{0.1}Gd_{0.9})(TTA)_3(TPPO)_2$ [16] could be obtained after pH adjustment with addition of NaOH solution, and another complex $Eu(DBM)_3(TPPO)$, where DBM is another β-diketone ligand dibenzoylmethide was reported in [17]. The existence of a water molecule in the lattice of complex **2** is caused by the requirement of the usual coordination number of 9 for Eu(III) and the smaller size of the nitrate ligand.

3.4. Luminescent properties

PL emission can be observed from complex **1** in powder state with the most intense peak at 645 nm and several minor peaks at 602, 564, 616 and 707 nm respectively (Fig. 5). However, compared to the Eu(III) ion, the Sm(III) ion is not an efficient emission center for organic light emitting devices. Hence, we have focused on the PL and EL properties of complexes **2** and **3** in thin film states in this study.

PL measurements were carried out on film samples of these two complexes obtained by vacuum evaporation. Fig. 6 shows the emission spectrum of complex **3**. An almost identical emission spectrum was obtained for complex **2**

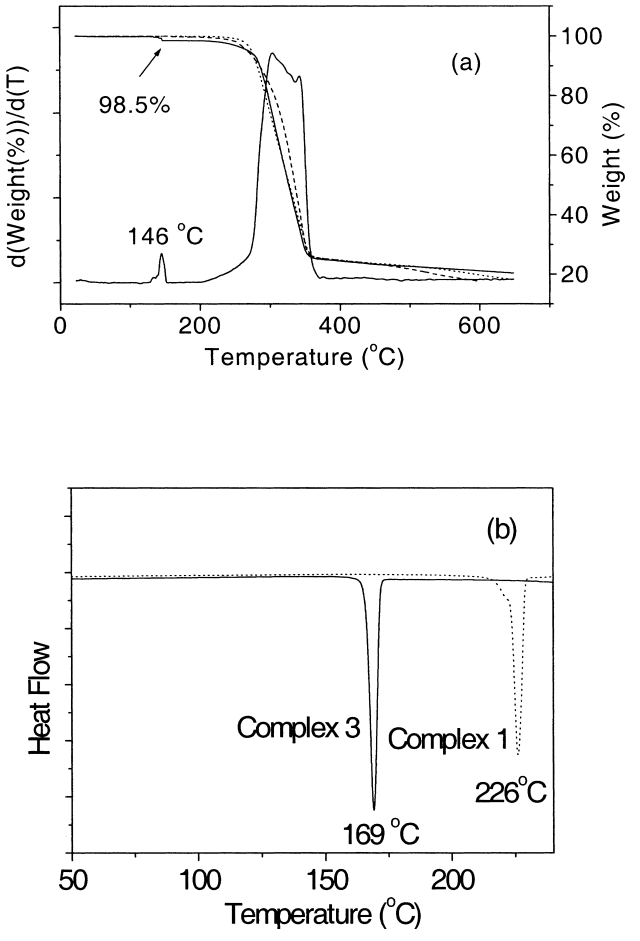

Fig. 4. (a) TGA curves of complexes **1** (dotted line), **2** (solid line) and **3** (dashed line). (b) DSC curves of complexes **1** (dotted line) and **3** (solid line).

(Fig. 7). The most intense and sharp emission at 615 nm should be assigned to the $^5D_2-^7F_2$ transition [11]. Other less intense emissions at 591, 534, 652 and 701 nm, are ascribed respectively to the $^5D_0-^7F_1$, $^5D_1-^7F_0$, $^5D_0-^7F_3$ and $^5D_0-^7F_4$ transitions. In spite of the identical emission

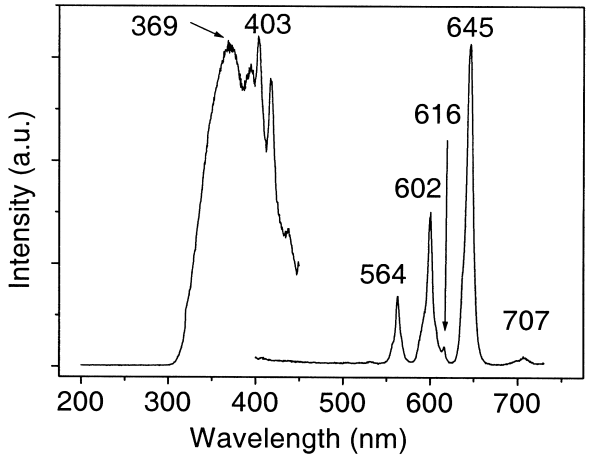

Fig. 5. PL spectra of complex **1** in powder state.

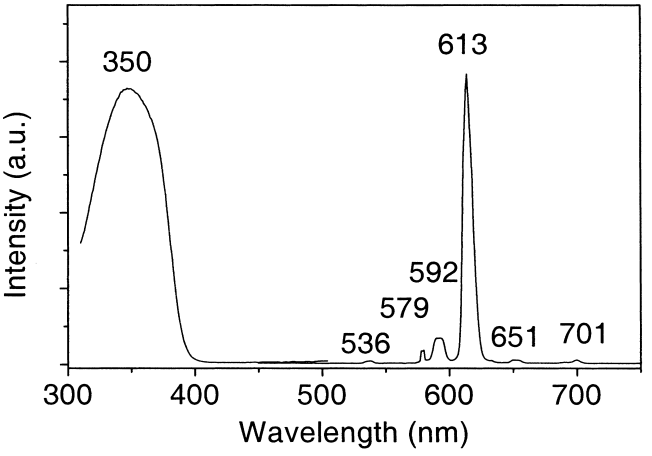

Fig. 6. PL spectra of complex **3** in film state.

spectra, the effects of composition difference between the complexes can be observed in the process of film deposition. In the case of complex **2**, some black residual remains without sublimation after the vacuum evaporation indicating that some kind of decomposition occurs with possible composition change, whereas for complex **3**, no black residual remains can be observed, i.e. no decomposition occurs in this case. As expected from the TGA and DSC results, complex **3**, which has a much lower melting point than complex **2** is much easier to be evaporated. These observations suggest that vacuum evaporation is more applicable to complex **3** than to complex **2** for the purpose of fabricating OLEDs.

Single layer devices of complex **2** were fabricated by vacuum evaporation. The EL spectrum is shown in Fig. 7 together with the PL emission spectrum of the evaporated film as a comparison. At low bias voltage, only an emission peak at 612 nm can be observed. As the bias voltage increases, other emission peaks appear at 534 and 460 nm. The 612-nm emissions can obviously be ascribed

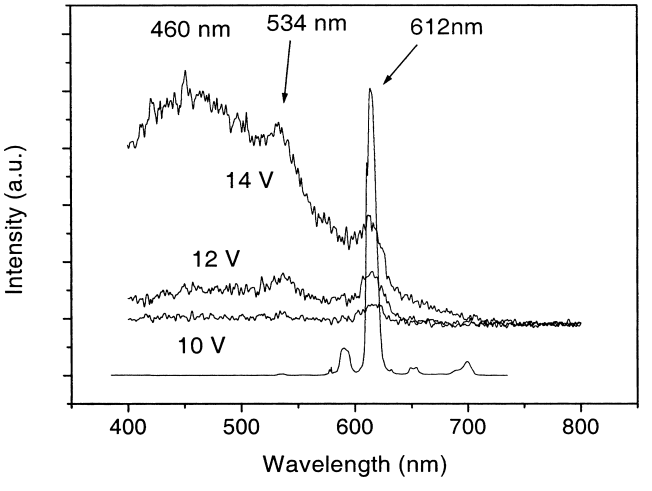

Fig. 7. EL spectra of a single layer device: ITO/complex **2** (40 nm)/Al and PL emission spectrum of complex **2**.

to complex **2**. The turn-on voltage is about 8 V. The low signal–noise ratio is caused by a low efficiency of carrier injection. An explanation of this can be made on the basis of the previously reported data on Eu(III) chelates. It was reported that in the rare earth complexes it is the β-diketone ligands that acts as the chromophore to absorb energy. Hence, the energy level values reported for similar complexes containing TTA can be referred to discuss the charge injection process (Fig. 8). Among TTA containing complexes, the lowest unoccupied molecular orbital (LUMO) and highest occupied molecular orbital (HOMO) of $Eu(TTA)_3phen$ was reported to be located at −3.1 and −6.3 eV with respect to the vacuum level [27]. Considering that the work function of ITO is in the range of 4.6–4.8 eV, we can deduce an energy barrier of more than 1.5 eV in the single layer device at the interface between ITO and complex **2**. This high value is the reason for the low efficiency of hole injection.

In order to improve hole injection efficiency, a hole transporting layer is needed. As reported [27], TPD has LUMO and HOMO values of −2.2 and −5.4 eV respectively. Thus if a TPD layer is inserted between the ITO and complex **2**, the injection barriers at the ITO/TPD and the TPD/complex **2** interfaces would be less than 0.8 and 0.9 eV respectively. Double layer devices with a TPD layer inserted in between the ITO and complex **2** were fabricated. As expected, double layer devices show improved emission performance compared with the single layer devices due to improvement in carrier injection balance and exhibit well-defined EL spectra with high signal–noise ratio (Fig. 9(a)). The most intense emission is at 612 nm as in the single layer device at low bias voltages. With increasing bias voltage, emissions at other wavelengths, such as 587 and 534 nm become relatively stronger. As a comparison, Fig. 9(a) also shows the EL emission spectrum for a single layer device (ITO/TPD (40 nm)/Al) with a peak at 403 nm. It is obvious that no emission from TPD can be observed from the double layer device, which should be around 410 nm. The turn on voltage of the double layer devices is about 10 V (Fig. 9(b)). This is 2 V higher than that of the single layer device and is caused by the increased thickness of the device layers.

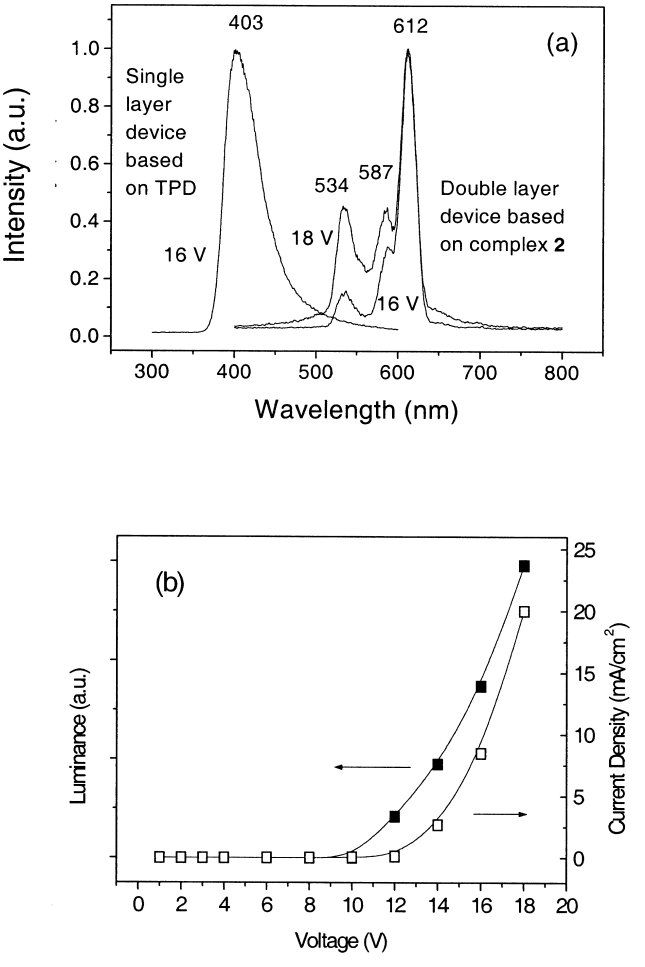

Fig. 9. EL properties of double layer device: ITO/TPD (40 nm)/complex **2** (40 nm)/Al. (a) EL spectra at different bias voltages with that of the single layer device ITO/TPD (40 nm)/Al as a comparison. (b) Dependence of luminance and current density on the bias voltage.

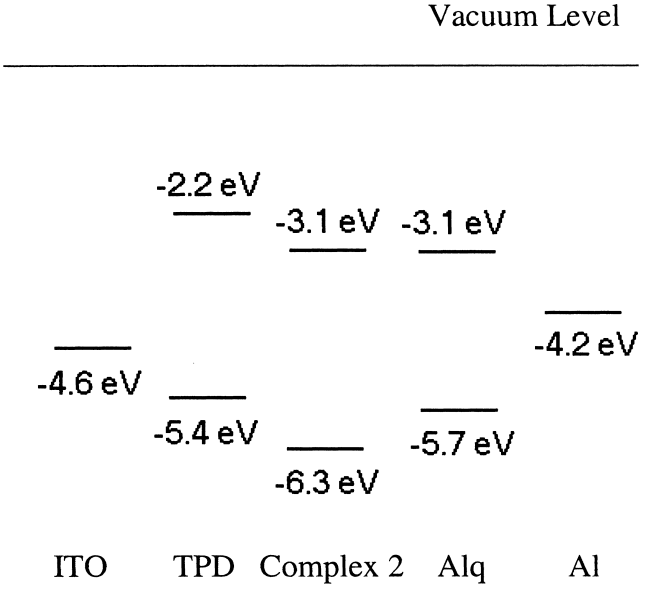

Fig. 8. Energy level diagram of three layer OLED device.

In the single layer device, the electrons injected from the Al cathode move to the lowest unoccupied molecular orbits (LUMO, −6.3 eV) of the complex and because of its electron transporting property they reach the interface where recombination occurs with holes injected from the ITO anode. The energy is transferred to the ligand sites of the complex where both singlet and triplet excitons form. The singlet excitons are converted into triplet excitons by intersystem crossing and are then transferred to the Eu(III) sites. In the double layer device, similar emission process occurs except that the hole injected from ITO first move to the highest occupied molecular orbits (HOMO) of TPD

(−5.4 eV) and the recombination happens at the interface between TPD and complex **2**.

Apart from the difference in intensity, a comparison between the EL spectra of single layer and double layer devices also shows that no emission can be observed at wavelengths less than 500 nm in the later case. Considering that in the single layer device the complex layer is evaporated directly onto the ITO surface, it is possible that some kind of interaction happens between the complex and the anode surface at higher bias voltage and causes additional emission peaks from the possible interfacial species.

In order to further improve the efficiency, electron transporting layer Alq was introduced to fabricate triple layer devices based on complex **2**. The results show that triple layer devices have EL spectra similar to the double layer devices. However, no significant improvement on emission intensity was observed (Fig. 10). Both the most intense emission at 615 nm and the two minor emissions at 587 and 537 nm should be emitted from complex **2**. Both TPD and Alq do not emit in this triple layer device and the role of the Alq electron transport layer is not so critical.

Fig. 11 shows the EL properties of double layer device based on complex **3**. The turn on voltage for luminance is about 14 V while it is about 4 V for current. It is anomalous that current density increases quickly with the increase of bias voltage at the beginning but drops before the bias voltage reaches the turn-on voltage for luminance. After the voltage reaches the luminance turn-on voltage, the current density remains constant while luminance increases rapidly with the increase of bias voltage. This phenomenon was observed in all measurements on devices fabricated in different attempts. The reason for this is not understood at present and further studies are being carried out.

For OLED devices, lifetime and packaging are important issues for applications. However, as mentioned in Section 2.2.3, the chelate complex EL devices were tested in the ambient without packaging being applied to seal the devices. This is because it is beyond the scope of this present study to investigate the lifetime and degradation issues of these OLED devices. As a result of exposure to moisture and oxygen, the device lifetime tend to be short. Qualitative observations have shown that degradation effects became significant within about 1 day. In order to minimize the effects of material degradation, the PL and EL measurements were typically carried out immediately after the devices were fabricated.

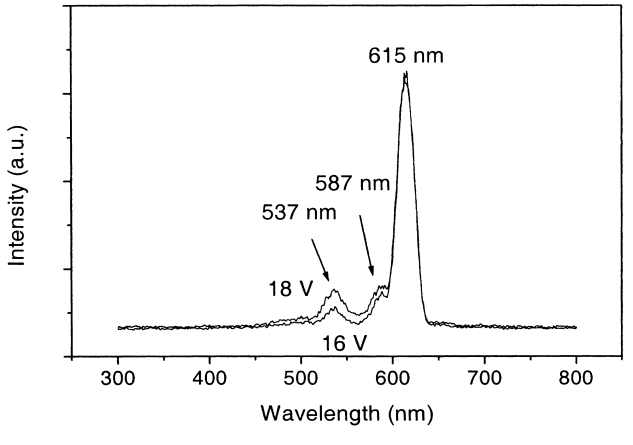

Fig. 10. EL spectra of triple layer device ITO/TPD (40 nm)/complex **2** (40 nm)/Alq (40 nm)/Al.

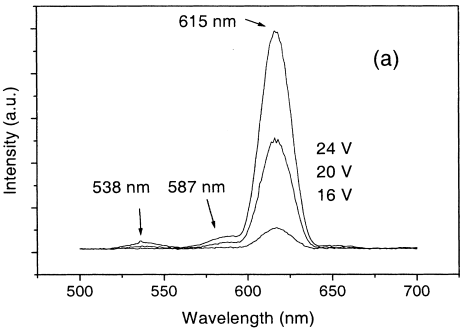

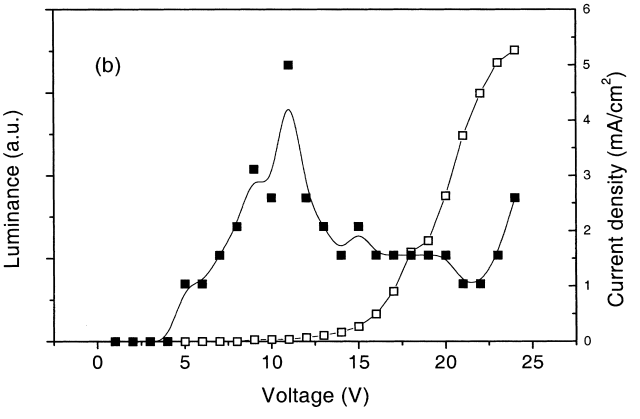

Fig. 11. EL properties of double layer device: ITO/TPD (50 nm)/complex **3** (60 nm)/Al.

4. Conclusions

Rare earth chelates were prepared using HTTA and TPPO as organic ligands with different rare earth salts. The compositions of complexes **1** and **2** prepared from Sm(III) and Eu(III) nitrate salts are $Sm(TTA)_2(TPPO)_2NO_3$ and $Eu(TTA)_2(TPPO)_2NO_3H_2O$ respectively with a nitrate donating two oxygen atoms coordinating to the central metals. The composition of complex **3** from Eu(III) acetate salt is $Eu(TTA)_3(TPPO)_2$. In these structures, Sm(III) shows a coordination number of 8 in complex **1**, while Eu(III) shows a different number of 9 and 8 in complexes **2** and **3** respectively. It is the acidity of the reaction solution and the steric effects of the ligands that determine the inorganic component percentage in the structures. All

the compounds exhibit strong photoluminescence and organic EL devices based on the chelates were fabricated. The single layer devices based on Eu(III) complex **2** can only emit weakly. Efficiency enhancement was observed with the introduction of a hole transporting layer (TPD) in the double layer device based on complex **2**. A triple layer device with an additional electron transporting layer (Alq) showed no improvement in efficiency compared to the double layer device. The vacuum evaporation of complex **3** is much easier than complex **2** with no residue after the evaporation process. The emission spectra from double layer devices are similar to those based on complex **2** with a maximum around 615 nm.

References

[1] C.W. Tang, S.A. VanSlyke, Appl. Phys. Lett. 51 (1987) 913.
[2] C.W. Tang, S.A. VanSlyke, C.H. Chen, J. Appl. Phys. 65 (1989) 3610.
[3] Y. Hamada, IEEE Trans. Electron Dev. 44 (8) (1997) 1208.
[4] C.H. Chen, J. Shi, Coord. Chem. Rev. 171 (1998) 161.
[5] M.R. Robinson, M.B. O'Regan, G.C. Bazan, Chem. Comm. 17 (2000) 1645.
[6] W. Zhu, Q. Jiang, Z. Li, X. Wei, M. Xie, D. Zou, T. Tsutsui, Thin Solid Films 363 (2000) 167.
[7] X.T. Tao, H. Suzuki, T. Wada, S. Miyata, H. Sasabe, J. Am. Chem. Soc. 121 (2000) 9447.
[8] A. Wu, D. Yoo, J.K. Lee, M.F. Rubner, J. Am. Chem. Soc. 121 (2000) 4883.
[9] N.X. Hu, M. Esteghamatian, S. Xie, Z. Popovic, A.-M. Hor, B. Ong, S. Wang, Adv. Mater. 11 (17) (2000) 1460.
[10] T. Jin, S. Inoue, K. Machida, G. Adachi, J. Alloys Comp. 265 (1998) 234.
[11] Y. Hamada, T. Sano, M. Fujita, T. Fujii, Y. Nishio, K. Shibata, Chem. Lett. 5 (1993) 905.
[12] P.E. Borrows, L.S. Sapochak, D.M. McCarty, S.R. Forrest, M.E. Thompson, Appl. Phys. Lett. 64 (20) (1994) 2718.
[13] Y. Hamada, T. Sano, M. Fujii, Y. Nishio, K. Shibata, Jpn. J. Appl. Phys. 32 (4A) (1993) L514.
[14] C.J. Liang, D. Zhao, Z.R. Hong, D.X. Zhao, X.Y. Liu, W.L. Li, J.B. Peng, J.Q. Yu, C.S. Lee, S.T. Lee, Appl. Phys. Lett. 76 (1) (2000) 67.
[15] X.C. Gao, H. Cao, C. Huang, B. Li, Appl. Phys. Lett. 72 (18) (1998) 2217.
[16] X. Zhang, R. Sun, Q. Zheng, T. Kobayashi, W. Li, Appl. Phys. Lett. 71 (18) (1997) 2596.
[17] W. Hu, M. Matsumura, M. Wang, L. Jin, Jpn. J. Appl. Phys. 39 (11) (2000) 644.
[18] Z. Hong, C. Liang, R. Li, W. Li, D. Zhao, D. Fan, D. Wang, B. Chu, F. Zang, L-S. Hong, S.T. Lee, Adv. Mater. 13 (16) (2001) 1241.
[19] C. Adachi, M.A. Baldo, S.R. Forrest, J. Appl. Phys. 87 (2000) 8089.
[20] M.D. McGehee, T. Bergstedt, C. Zhang, A.P. Saab, M.B. O'Regan, G.C. Bazan, V.I. Srdanov, A.J. Heeger, Adv. Mater. 11 (16) (1999) 1349.
[21] J. Kido, H. Hayase, K. Hongawa, K. Nagai, K. Okuyama, Appl. Phys. Lett. 65 (1994) 2124.
[22] W.L. Li, J.Q. Yu, G. Sun, Z. Hong, Y. Yu, Y. Zhao, J.B. Peng, T. Tsutsui, Synth. Met. 91 (1997) 263.
[23] S. Capecchi, O. Renault, D.-G. Moon, M. Halim, M. Etchells, P.J. Dobson, O.V. Salata, V. Christou, Adv. Mater. 12 (21) (2000) 1591.
[24] N. Sabbatini, M. Guardigli, J.-M. Lehn, Coord. Chem. Rev. 123 (1993) 201.
[25] G.M. Sheldrick, SHELXTL PC, Version 5.03, Siemens Analytical X-ray Instruments Inc., Madison, WI, USA. 1994.
[26] H.D. Flack, Acta Crystallogr. A39 (1983) 876.
[27] Y. Ohmori, H. Kajii, T. Sawatani, H. Ueta, K. Yoshina, Thin Solid Films 393 (2001) 407.